

Contents — E through G

Bushveld Complex, South Africa: Impact and Plume Models Reconciled <i>W. E. Elston</i>	4032
Experimental Simulation of Shock Reequilibration of Fluid Inclusions During Meteorite Impact <i>M. E. Elwood Madden, F. Hörz, and R. J. Bodnar</i>	4013
Weaubleau-Osceola Structure, Missouri: Deformation, Event Stratification, and Shock Metamorphism of a Mid-Carboniferous Impact Site <i>K. R. Evans, C. W. Rovey II, K. L. Mickus, J. F. Miller, T. G. Plymate, and K. C. Thomson</i>	4111
Transformation of Some Minerals in Shock Waves — Comparison of Natural and Experimental Data <i>V. I. Fel'dman, L. V. Sazonova, E. A. Kozlov, and Ju. N. Zhugin</i>	4014
Chemical Differentiation of Impact-produced Melt Droplets: Experiments and Observation <i>M. V. Gerasimov, O. I. Yakovlev, Yu. P. Dikov, and F. Wlotzka</i>	4089
New Data on the Late Pliocene Eltanin Impact into the Deep Southern Ocean <i>R. Gersonde, F. T. Kyte, T. Frederichs, U. Bleil, and G. Kuhn</i>	4094
Reports of Discovery of the “Eltanin Crater” are Contradicted by Data <i>R. Gersonde, F. T. Kyte, T. Frederichs, U. Bleil, and G. Kuhn</i>	4095
Vredefort 2003 — Recent Progress, New Challenges <i>R. L. Gibson, W. U. Reimold, and C. Lana</i>	4082
Magnetic Fabric Studies of the Whistle and Parkin Offset Dykes from the Sudbury Impact Structure <i>L. A. Giroux and K. Benn</i>	4103
Active Seismic and Drilling Studies of the Chicxulub Impact Crater: A Status Report <i>S. P. S. Gulick, G. L. Christeson, J. V. Morgan, M. R. Warner, P. Barton, J. Urrutia-Fucugauchi, and H. J. Melosh</i>	4019

BUSHVELD COMPLEX, SOUTH AFRICA: IMPACT AND PLUME MODELS RECONCILED. W. E. Elston, Department of Earth and Planetary Sciences, University of New Mexico, Albuquerque, NM 87131-1116, U.S.A., weelston@earthlink.net.

Introduction: The (unpopular) impact model for the Bushveld Complex [1, 2] is based on evidence for an initial catastrophe, preserved in extraordinary high-temperature, high-energy debris flows at the base of its oldest unit (Rooiberg Group, ~2,061 Ma) and on intense deformation bracketed between the end of pre-Bushveld marine sedimentation and the coming-to-rest of the basal debris flows. The alternative (popular) mantle plume model [3, 4] is based on a long sequence of subsequent events related to sequential partial melting of mantle and crust: Evolution of the Rooiberg Group from diverse predominantly mafic flows to homogeneous siliceous flows of increasingly conventional volcanic aspect, overlapping with intrusion (into the base of the Rooiberg Group) and quiet differentiation of massive mafic cumulate sills (Rustenburg Layered Suite, *RLS*), followed by sills of A-type granite (Lebowa Granite Suite, *LGS*). The hydrodynamic model of Jones et al. [5] for an impact-triggered long-lived mantle plume promises to reconcile the two Bushveld models. It cites the Bushveld Complex as a possible example of a large igneous province generated by decompression melting at the leading edge of a shallow mantle plume, triggered by impact of an iron bolide ($d \geq 20$ km, $v \geq 10$ km/sec).

Plume Criteria: Jones et al. [5] distinguished shallow impact-triggered (I-type) plumes rooted in the upper mantle from endogenic hot-spot (H-type) plumes, deeply rooted at the core-mantle boundary. The Bushveld Complex meets their criteria for a large igneous province generated by an I-plume: Melt volume $\geq 10^6$ km³, crater "auto-obiterated" by melts, high rate of eruption, no initial doming, "plume-like geochemical signature," "no deep geophysical fingerprint." A modest modification involves substituting mafic flows in the lower 2,000 m of the Rooiberg Group for initial "low-viscosity peridotitic melts."

Distinctiveness of the Bushveld Complex: In its early impact-dominated stage, the Bushveld Complex conformed generally to the to a model developed for Chixculub [6]. It is proposed that three quasi-simultaneous impacts resulted in (i) an outward-collapsed central peak, (ii) a melt sheet inside a three-lobed transient cavity, ~150 km in diameter, surrounded successively by (iii) a peak ring and zone of inward collapse, (iv) a deep three-lobed basinal outer ring, 250-km diam. (=ring syncline [1]) and (v) a 400-km diam. exterior ring (= ring anticline [1]; = chain of uplifts [7]). The Bushveld then diverged from the Chixculub model during the I-plume stage. As pre-

dicted, intrusions by crustal melts of LGS granite auto-obiterated the transient cavity except for two 50-km windows, in which segments of its wall are exposed. The Bushveld Complex and two other proposed Proterozoic multi-ring impact structures, Vredefort and Sudbury, can be interpreted as a denudation series: Vredefort has been eroded to the sub-crater basement. Only dikes injected into the basement remain of its melt sheet [8]; no ejecta remains in its ring basins. Sudbury preserves basement and a segment of crater floor, melt sheet and impactite crater fill. No outflow is preserved in the ring basins. In the Bushveld Complex, the Rooiberg Group and RLS are entirely preserved in the basinal outer ring, with a maximum thickness (including LGS) of ~12 km. No crater fill, crater floor, or basement has been documented to date. The Bushveld Complex is topless; its earliest member, the Rooiberg Group caps subsequent RLS and LGS sills. A 300-km westward RLS tail, ending in the buried Molopo Farms Complex (Botswana), suggests that the plume was affected by a deep E-W lineament. A small RLS outlier, the Losberg body, lies in a ring of the Vredefort impact structure, 100 km to the south.

The Impact Stage: Evidence for the proposed impact is seen in the two windows exposing the transient cavity wall. They are located, respectively, in the eastern and western Bushveld lobes. Each consists of two *fragments*, in fault contact: *deformed*, interpreted in terms of the outward collapse of a central peak; and *undeformed*, interpreted by inward collapse of the unstable walls of an enlarging transient cavity.

Deformed fragments. In the deformed fragments, pre-Bushveld rocks (Transvaal Supergroup), intensely sheared, tightly (even isoclinally) folded and metamorphosed to pyroxene hornfels facies [9], are interpreted as segments of a collapsed central peak [6], ramped against the cavity wall. Deformation of this intensity is not known elsewhere in the Transvaal Supergroup or worldwide in any volcanic setting.

Undeformed fragments. In the studied eastern undeformed (Stavoren) fragment, unmetamorphosed and unfolded Transvaal quartz-sericite arenite is cut by breccia zones and overlain by tens of meters of an unbrecciated basal Rooiberg debris flow. The debris flow superficially resembles rhyolite studded with m-size quartzite xenoliths in every stage of deformation, recrystallization, and dissolution. In petrography and chemistry, its matrix turns out to be comminuted and partially melted quartz-sericite arenite. The rock, of local and shallow provenance, is interpreted as derived

from the overturned crater rim. Its quartz grains inverted in the solid state into ordered and disordered forms of high-tridymite [10]. Late-stage tridymite needles to 5 mm crystallized directly from quenched interstitial melt. Although larger, they resemble needles in a 60-m quartzite breccia at the base of Onaping impactite at Sudbury [11]. In a >10 m metamorphic zone below the debris flow, quartzite inverted to massive tridymite. On cooling, all forms of tridymite inverted back to paramorphous quartz. The entire sequence is unknown in volcanic environments. The closest analogs to the solid-state inversions occur in silica-brick furnace linings, heated to 1,200-1,370°C [12]. Further evidence for extraordinary temperatures comes from the absence of zircon [13] in transformed arenite with 191-304 ppm Zr. Melting and high-T low-P sanidinite-facies metamorphism account for the absence of high-P SiO₂ polymorphs and PDFs.

Origin of the undeformed fragments. The undeformed fragments are interpreted as gigantic gravity slide blocks that encountered debris flows on their way into the enlarging transient cavity. At the strike-slip fault contact with the neighboring deformed (Marble Hall) fragment, the Stavoren fragment broke into overturned quartzite slabs, tens to hundreds of meters long, that became engulfed in the debris flow.

Other debris flow occurrences. Aside from the undeformed fragments, the basal debris flows of the Rooiberg Group have generally been destroyed by metamorphism and rheomorphic melting at contacts with intruding RLS and LGS sills. Only along the SE margin of the Bushveld Complex (Dullstroom area) was a 2,000-m slice of Rooiberg rocks preserved beneath the RLS. At their base, up to 300 m of debris flows were preserved in three (scoured?) paleochannels [14]. Inflated hot flows deposited sand-size quartz grains in a fine mafic matrix, cm-size lithic clasts metamorphosed *in situ* to amphibolite hornfels, and m-size blocks of shattered quartzite. An ignimbrite-like transport mode is indicated by basal surge deposits, lag deposits of boulder-size clasts, and an interlayered mafic ash-cloud deposit. Overlying rhyolite-like lavas consist of the same material, melted.

The I-Plume Stage: The I-plume dominated the well-documented petrochemical evolutions of the Rooiberg Group above the basal debris flows, RLS and LGS (3, 4, 15, 16). The initial melt sheet was augmented by partial decompression melts from the head of the rising plume. As a result of explosions triggered by periodic influxes of water, up to 4.5 km of Rooiberg rheoignimbrite flows, interlayered with high-energy sedimentary and pyroclastic deposits, accumulated in the basinal outer ring. Based on the Chixculub model [6], an inward-dipping fault from the outer ring

to the Moho may have acted as a conduit for RLS mantle melts contaminated with crustal material. They formed sills up to 9 km thick at the base of the Rooiberg Group, as late-stage siliceous Rooiberg flows continued to pile on top. Those RLS sills that yielded consistent paleomagnetic orientations were horizontal at the time of crystallization (17). Collapse to form the present three Bushveld basins may have coincided with emplacement of sills of LGS crustal melts, up to 5 km thick, into basin fill and the Rooiberg-RLS contact. LGS granite nearly engulfed the undeformed fragments, probably by invading the soles of the slide blocks. Subsidence of the basins tilted RLS sills into present inward-dipping positions and rotated their feeders closer to vertical. The outward-verging recumbent folds of the deformed fragments rotated toward the vertical and the outward-dipping undeformed fragments toward the horizontal. Collapse may have been the cause of a second catastrophe, recorded in the upper part of the Rooiberg Group. It emplaced megabreccia blocks up to 50 m around the entire circumference of the Bushveld Complex [1, 18]. The blocks, and mm-sized xenoliths in their ignimbritic matrix, show moderate shock effects (cataclasis, deformation twins and lamellae, *not* PDFs). Spherules, mm sized, formed in this stage and are also imbedded in the matrix. Minor siliceous magmatism and structural adjustments continued into post-Bushveld time.

References: (1) Rhodes, R. C. (1975) *Geology*, 3, 549-554. (2) Elston, W. E. (1996) *Met. & Planet. Sci.*, 31, Suppl. A42. (3) Hatton, C. J. and Schweitzer, J. K. (1995) *S. Af. J. Geol.*, 98, 245-255. (4) Buchanan, P. J., et al., (1999) *Cont. Min. Pet.*, 137, 133-146. (5) Jones, A. P., et al. (2002) *E. & P. S. Letters*, 202, 551-561. (6) Morgan, J. V. et al. (2000) *E. & P. S. Letters*, 5660, 1-8. (7) von Gruenewaldt, G. (1979) *Can. Min.* 17, 233-256. (8) Buchanan, P. J. & Reimold, H. U. (2002) *Met. & Planet. Sci.* 37, 807-822 (9) Hartzler, F. (1994) *Ph.D. diss., Rand Afrikaans U.*, 363 p. (10) Flörke, O. W. et al. (1988) *N. Jb. Min. Abh.*, 158, 175-182. (11) Stevenson, J. S. (1963) *Can. Min.*, 7, 413-419. (12) Schneider, H. and Flörke, O. W. (1982) *N. Jb. Min. Abh.* 145, 280-290. (13) Harmer, J. and Farrow, D. (1995), *Mineral. Deposita*, 30, 188-195. (14) Schweitzer, J. K. (1998) *Unpub. Ph.D. diss., U. Pretoria*, 20 p. +10 Append. (15) Schweitzer et al. (1997) *J. Af. Earth Sci.*, 24, 95-104. (16) Twist, D. (1985) *Econ. Geol.* 80, 1153-1165. (17) Hattingh, P. (1998) *S. Af. Geophys. Rev.* 2, 75-77. (18) Schweitzer et al., 1995, *S. Af. J. Geol.* 98, 245-255.

EXPERIMENTAL SIMULATION OF SHOCK REEQUILIBRATION OF FLUID INCLUSIONS DURING METEORITE IMPACT. M.E. Elwood Madden¹, F. Hörz², and R.J. Bodnar³ ¹Dept. of Geological Sciences, Virginia Tech, Blacksburg, VA 24060, melwood@vt.edu, ²NASA Johnson Space Center, Houston, TX 77058. ³Dept. of Geological Sciences, Virginia Tech, Blacksburg, VA 24060, bubbles@vt.edu.

Introduction: Fluid inclusions are microscopic volumes of fluid trapped within minerals as they precipitate. Fluid inclusions are common in terrestrial minerals formed under a wide array of geological settings from surface evaporite deposits to kimberlite pipes [1]. While fluid inclusions in terrestrial rocks are the rule rather than the exception, only a few fluid inclusion-bearing meteorites have been documented [2],[3],[4],[5]. The rarity of fluid inclusions in meteoritic material may be explained in two ways. First, it may reflect the absence of fluids (water?) on meteorite parent bodies. Alternatively, fluids may have been present when the rock formed, but any fluid inclusions originally trapped on the parent body were destroyed by the extreme P-T conditions meteorites often experience during impact events. Distinguishing between these two possibilities can provide significant constraints on the likelihood of life on the parent body.

Just as textures, structures, and compositions of mineral phases can be significantly altered by shock metamorphism upon hypervelocity impact, fluid inclusions contained within component minerals may be altered or destroyed due to the high pressures, temperatures, and strain rates associated with impact events. Reequilibration may occur when external pressure-temperature conditions differ significantly from internal fluid isochoric conditions, and result in changes in fluid inclusion properties and/or textures (Figure 1). Shock metamorphism and fluid inclusion reequilibration can affect both the impacted target material and the meteoritic projectile. By examining the effects of shock deformation on fluid inclusion properties and textures we may be able to better constrain the pressure-temperature path experienced by shocked materials and also gain a clearer understanding of why fluid inclusions are rarely found in meteoritic samples.

Methods: Disks containing numerous (>100) two-phase (liquid + vapor bubble) aqueous fluid inclusions of varying size and shape and with similar liquid:vapor ratios were cut from Arkansas quartz crystals, polished and documented optically. The homogenization temperatures of the fluid inclusions were measured in 20K steps using a USGS-type heating stage [1]. Pre-impact fluid inclusion homogenization temperatures ranged from 373 to 433K with the mode lying between 393 and 413K in all the disks.

The documented quartz disks were subjected to 5-30 GPa Flat Plate Accelerator experimental impacts

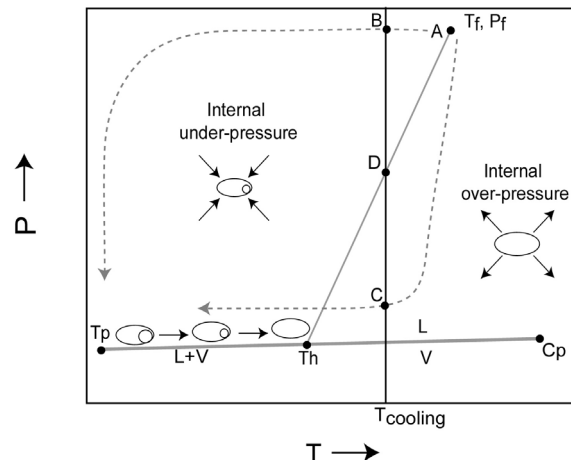


Figure 1: Pressure-temperature conditions inside a fluid inclusion as a function of temperature and pressure. The liquid-vapor curve is labeled L+V and extends from the triple point (Tp) to the critical point (Cp). The fluid inclusion isochores extends from the homogenization temperature (Th) to the fluid inclusion trapping conditions (Tf, Pf). At any temperature (T) the pressure inside of a fluid inclusion is defined by the pressure along the liquid-vapor curve (before homogenization occurs) or along the fluid isochores (after the inclusion homogenizes). A fluid inclusion trapped at conditions Tf, Pf (point A) whose P-T cooling or uplift path corresponds to the fluid isochores (D) will always maintain the same pressure inside of the inclusion as outside, therefore the inclusion will not reequilibrate since there is no pressure gradient. If, however, the sample containing the fluid inclusion follows an initial isobaric cooling path (through B), the external pressure is always greater than the internal pressure and reequilibration due to the internal under-pressure may occur. The resulting decrease in the volume of the fluid inclusion produces an increase in fluid density and a decrease in homogenization temperature. If the rock follows an isothermal uplift path (C), the fluid inclusion may reequilibrate owing to internal over-pressures, resulting in an increase in the size of the fluid inclusion, a decrease in fluid density, and an increase in homogenization temperature.

at NASA's Experimental Impact Laboratory following the procedure of [6]. The shocked disks were then re-polished and documented. If fluid inclusions were found within the shocked samples, their homogenization temperatures were again measured. By comparing the pre- and post-impact fluid inclusion data, the effects of shock reequilibration were qualitatively (textures) and quantitatively (homogenization temperatures) observed.

Results: The results obtained here show that fluid inclusion textures undergo a systematic and gradual evolution with increasing, albeit modest (5-10 GPa), shock pressures (Table 1). At the lowest shock pressures (5-6 GPa), the most common type of

reequilibration is slight stretching of the inclusion volume, as evidenced by $\sim 20\text{K}$ increase in post-shock homogenization temperatures (range 393-453K, mode 493-413K). With increasing shock pressure, fluid inclusion reequilibration is dominated by decrepitation (with complete loss of the fluid from the inclusion to produce an empty cavity). At higher shock pressures (8.4-10 GPa) the fluid inclusions have completely collapsed. At shock pressures near or above the Hugoniot elastic limit, reequilibration is characterized by the complete disappearance of any preexisting fluid inclusions (see [7] for more detailed observations).

Results of these experiments suggest that fluid inclusions undergo a decrease in volume (collapse) within the first few microseconds following impact as the shock wave moves through the sample, producing a relatively high pressure external environment compared to the lower pressure in the inclusion (Figure 2). If the fluid inclusions survive this event, the initial volume decrease is overprinted by stretching due to internal overpressures experienced during sustained high temperature conditions as the decompressed rocks cool following the shock event. This portion of the P-T cycle leads to an increase in inclusion volume and homogenization temperature and, possibly, decrepitation.

Conclusions: The experimental results suggest that fluid inclusion textures may provide constraints on the maximum shock pressure experienced by the sample. These results also indicate that the absence of fluid inclusions in meteoritic materials does not preclude the presence of fluids on meteorite parent bodies-- instead relatively modest shock processes may have destroyed all previously trapped fluid inclusions.

Acknowledgements: Thanks to Craig Altare for help with sample preparation. This work was partially supported by NSF Grant EAR-0125918 to R.J. Bodnar.

References: [1] Roedder (1984) *Fluid Inclusions* [2] Bodnar (1999) *LPS XXX*, 1222 [3] Zolensky et al. (1999) *Science* 285, 1377-1379. [4] Rubin et al. (2002) *Meteorit. Planet. Sci.* 37, 125-141. [5] Bridges and Grady (2000) *Meteorit. Planet. Sci.* 35, 33-34. [6] Skala et al. (2002): *Geol Soc Am Spec Paper* 356, 571-585. [7] Elwood Madden et al. (2003) *Can.Min* in review. [8] Gratz et al. (1992) *Phys Chem of Min* 19, 267-288.

Table 1: Summary of Results

Shock Pressure (GPa)	Fluid Inclusion Evidence
5.0	FI's present Th increase $\sim 20\text{K}$
6.0	FI's present Th increase $\sim 20\text{K}$ Decrepitated FI's Collapsed FI's
7.6	Decrepitated FI's Collapsed FI's
8.4	Collapsed FI's
10.0	Collapsed FI's
12.4	Possible Collapsed FI's
18.0	No FI textures
24.2	No FI textures
30.8	No FI textures

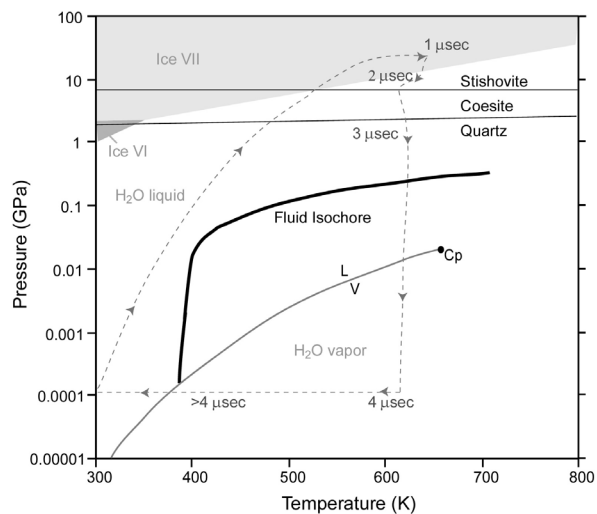


Figure 2. Pressure-temperature-time path followed by quartz during a 22 GPa experimental (small sample scale) impact event. The dashed gray line with arrows approximates the P-T path of the sample [8]. Note that for the first 3 μsec after impact, the fluid inclusions experience a significant internal under-pressure (P-T path is above the fluid isochore) and ice VII may be formed within the inclusions. The quartz host also passes through the coesite field and into the stability field of stishovite during this event. After 3 μsec , the high pressure shock wave has traveled through the sample and the pressure returns to ambient conditions, however the temperature of the sample remains high for an extended period as the quartz slowly cools, resulting in an extended period of internal over-pressure within the fluid inclusions (the P-T path is below the fluid isochore).

WEAUBLEAU-OSCEOLA STRUCTURE, MISSOURI: DEFORMATION, EVENT STRATIFICATION, AND SHOCK METAMORPHISM OF A MID-CARBONIFEROUS IMPACT SITE. K. R. Evans, C. W. Rovey II, K. L. Mickus, J. F. Miller, T. G. Plymate, and K. C. Thomson, *Department of Geography, Geology, and Planning, Southwest Missouri State University, Springfield, MO 65804-0087 (email: kre787f@smsu.edu)*

Introduction: The Weaubleau-Osceola Structure in southwestern Missouri is a newly recognized 19-km-diameter circular feature that includes deformed Mississippian and older strata overlain by an event breccia and undeformed Pennsylvanian siliciclastic strata (Fig. 1). Recent discoveries of planar fractures and planar deformation features (pdf) in quartz from various breccia facies, variably oriented shatter-cone-like striae in deformed strata, and coincidence of a low-gravity anomaly support the idea that it is a meteorite impact site.

The Weaubleau structure *sensu* Beveridge [1] is one of several 38th parallel structures across mid-continental North America that have figured prominently in the endogenic-exogenic controversy [2-4], but since efforts during the 1950's and 1960's only reconnaissance-level geologic mapping studies have been initiated. Our new investigations follow the discovery of the large circular drainage basin and radial tributaries that are noticeable in a digital elevation model of the area surrounding the Weaubleau structure. Although it is much smaller, the drainage pattern bears striking resemblance to the Manicouagan impact of Quebec.

A New Name. The name "Weaubleau structure" originally referred to Weaubleau Creek, which runs through the middle of the structure, but because of the larger scope and paradigm shift in our understanding of its origin, we prefer to use the name "Weaubleau-Osceola structure". This structure is unique among the 38th parallel impacts because shortly after the event, the structure was buried near the feather edge of the Pennsylvanian, and it has been only partly exhumed by modern erosion. Consequently, it is remarkably well preserved, and a suitable candidate for precise relative age-dating based on fauna and geochemical signatures of the event bed and correlative strata in nearby areas.

Morphology: Based on existing mapping and drilling records, it is likely that the central 19-km circular feature marks the limits of the transient crater. Outside of this structure in two narrow areas, Mississippian strata have been eroded and Lower Ordovician strata have been uplifted and truncated at the base of the Pennsylvanian. We interpret these features as part of a relict crater rim, however, sub-Pennsylvanian karstification and channel cutting greatly modified the crater morphology.



Figure 1. Digital elevation model of the Weaubleau-Osceola structure shows a relict circular depression that outlines the transient crater. Although the uppermost target rocks are Mississippian carbonates, uplifted areas of Lower Ordovician dolomite that we interpret as relict parts of the crater flank the southwestern and northeastern margins and are beveled below the sub-Pennsylvanian unconformity.

Stratigraphy: The youngest highly deformed strata (target rock) exposed in the structure are the Burlington-Keokuk and Pierson formations undivided (Osagean); these units are dominantly crinoid grainstone to packstone interbedded with chert.

The Northview Formation (Kinderhookian), a green-gray siltstone unit, generally is found below the Pierson Formation in this region [5], but within the structure, it is partly missing. Underlying beds of the Sedalia and Compton formations (Kinderhookian) are dominantly mud-rich carbonates. All of these strata lie unconformably over the Lower Ordovician Jefferson City-Cotter Dolomite undivided. These rocks are the lowest rocks exposed in this area.

Structural Deformation: Three distinct structural domains in the Burlington-Keokuk-Pierson lithosome

are exposed in walls of the Ash Grove Aggregate Quarry near the center of the structure, 7 km southeast of Osceola. The uppermost level is so heavily fractured that it is difficult to determine bedding and offset along faults. A second middle-level domain consists of tight folds and thrust faults along thin shale and silt-rich decollement surfaces (Fig. 2). Shale and siltstone are rare in the Burlington-Keokuk-Pierson formations but fine siliciclastic material from underlying strata of the Northview Formation may have provided a ready source of lubrication of movement along faults. Discrete zones of mixed carbonate and siliciclastic injection breccia, with gray-green siltstone clasts commonly are intermingled with folded strata. The absence of Northview Formation to the southwest and common occurrence of siliciclastic material in the dominantly carbonate target strata suggests that the fluidization and injection of siliciclastic material was virtually instantaneous among the brittle and plastically deformed carbonates. Reconnaissance-level field studies of z-folds, recumbent folds, and imbricate thrusts indicate movement toward the north. Only the upper part of the lower domain is exposed in the quarry. These strata are gently folded carbonates. Thus, the intensity of deformation decreases downward, indicating that the deformation originated above the present bedrock surface.



Figure 2. Large, tight folds and thrust fault of the middle-level structural domain in quarry near Osceola, Missouri.

Event Stratification: A mixed carbonate and siliciclastic breccia overlies deformed carbonates. We informally refer to this unit as the "Weaubleau Breccia." It is a polymict breccia with carbonate mudstone matrix and pebble-sized and larger angular and red-discolored chert clasts and angular clasts of siltstone and shale. The unit is matrix supported, poorly sorted and grossly stratified in a massive bed. Submillimeter-scale octahedra of hematite and goethite (after magnet-

ite?) are finely disseminated through the matrix. Locally, chert concretions are formed around larger siltstone clasts. The unit contains fauna and clasts ranging from at least Early Ordovician to Middle Mississippian.

Matrix support, lack of regular bedding, and the angular clasts of soft shale preclude fluvial transport of clasts. We interpret this unit as a fall-back impact breccia.

Shock Metamorphism: Mechanical twinning is ubiquitous in carbonate clasts in the breccia. A gradient exists between variably oriented stylolites to convergent pressure-solution striae that resemble horse-tailing, however no definitive shatter cones have been found. Approximately 10% of the coarse quartz sand exhibit multiple sets of parallel fractures and pdf's that remain unindexed (Fig. 3). Shocked quartz grains commonly are "toasted" with a semi-opaque yellow-brown appearance.

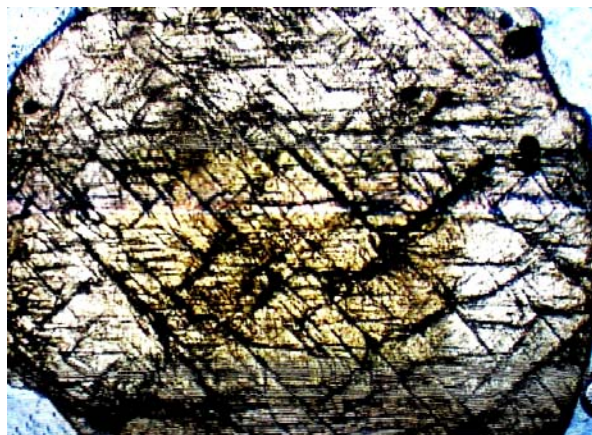


Figure 3. Photomicrograph shows planar fractures and faintly visible pdf's. Grain diameter is approximately 1.5 mm.

Conclusion: Based on available evidence, we consider that the Weaubleau-Osceola structure is an impact site. It tentatively appears to be terminal-Osagean in age, a biochronostratigraphic horizon that elsewhere marks the extinction of several echinoderm genera and species in North America.

References: [1] Beveridge T. R. (1951) *Mo. Geol. Surv. Water Res.*, 32, 2nd Ser. 111 pp. [2] Snyder F. G. and Gerdemann P. E. (1965) *Am. Jour. Sci.*, 263(6), 465-493. [3] Rampino M. R. and Volk T. (1996) *Geophy. Res. Lett.*, 23, 49-52. [4] Luszczaj J. (1998) *Geology*, 26, 295-298. [5] Thompson T. L. (1986) *Mo. Dept. Nat. Res. Div. Geol. And Land Surv., Rept. Inv.* 70, 182 pp.

TRANSFORMATION OF SOME MINERALS IN SHOCK WAVES – COMPARISON OF NATURAL AND EXPERIMENTAL DATA.

V.I.FEL'DMAN*, L.V.SAZONOVA*, E.A.KOZLOV**, Ju.N.ZHUGIN**

*M.V.Lomonosov Moscow State University, Geological Faculty, Department of Petrology, Moscow, 119899, Russia. E-mail: feldman@geol.msu.ru

**Russian Federal Nuclear Center - Zababakhin Institute of Technical Physics, Snezhinsk, box 245, 456770, Russia. E-mail: tagor@onti.ch70.chel.su

There are some differences in natural and experimental shock-thermal aggregates (STA) in minerals of target rocks.

For comparing the transformations of a matter in shock waves under natural meteoritic impact conditions and loading of a matter by spherical converging shock waves, the data on the Janisjarvi astrobleme and the on experiments with the rocks of its target have been used.

The Janisjarvi astrobleme (Karelia, Russia) has the diameter of 16 km and K - Ar age equal to 700 ± 5 million years. The geology of this structure and the shock metamorphism of the target rocks have been studied in detail [1 - 6]. For experiments the plagioclase-binary mica - quartz schist with garnet and staurolite have been chosen. A sample was made in the form of a ball, that have 49 mm in diameter, was welded up in a steel hermetic jacket and then was subjected to loading by a spherical convergent detonation wave of the HMX-based explosive composition layer at the external radius of the explosive layer equal to $R_{exp} = 40$ mm and its thickness $h_{exp} = 10$ mm [7]. The load amplitudes realized in a ball were changed from 25 GPa on its surface to 300 GPa on the radius of 1 mm. The loading impulse duration amounted to 1-2 μ s. In the process of the shock wave loading in the sample center, the ellipsoidal zone of melt has occurred, whose sizes in the meridional section were equal to 3×3.5 mm.

The comparative investigation of shock metamorphism of rocks made it possible to establish the following its features.

1. Sequence of the shock-thermal decomposition of colored minerals in nature and experiment coincide completely. First biotite begins to be destroyed (at about 20.0 GPa), then staurolite follows (21.0 - 25.0 GPa) and, at last, garnet (at 25.0 - 32.0 GPa). The character of migration of the components in stress waves is also the same.

2. Differences consist in the composition of STA. In nature STA in staurolite are formed from rhombic pyroxene, hercynite and sanidine. The parameters of forming these aggregates have been estimated to be equal about 20.0 GPa and 600°C [4]. In the experiment, STA include corundum and sometimes hercynite and glass. These differences are an indication of the more high-temperature character of STA in the experiment. From the equilibrium phase diagram of $\text{SiO}_2 - \text{Al}_2\text{O}_3 - \text{FeO}$ [8] it follows that the corundum crystallization is possible in the interval of 2000 - 1700°C after that it is substituted by hercynite and then by mullite. In our case hardening of the residue into glass takes place prior to the mullite occurrence, i.e. temperature was no lower than 1600°C. If σ_{xx} is estimated for these residual temperatures (postshock temperatures) according to the curve $\sigma_{xx} - T^{\circ}_{\text{postshock}}$ for quartz [9], then σ_{xx} is found within the range of 55.0 - 40.0 GPa. In nature, STA in biotite composed by rhombic pyroxene, ilmenite and glass are formed (with the same parameters that are shown above for staurolite). In the experiment, STA consist of ringwoodite, hercynite and glass in biotite [10]. At the same time ringwoodite contains up to 13 - 14% of Al_2O_3 . By using phase diagrams of $\text{SiO}_2 - \text{Al}_2\text{O}_3 - \text{FeO}$ and $\text{SiO}_2 - \text{Al}_2\text{O}_3 - \text{MgO}$ [8], the temperature of the ringwoodite (as analog of olivine) and rhombic pyroxene crystallization onset is estimated to be equal to 1600 - 1500°C and σ_{xx} (similarly to staurolite) approximately equals to 21.0 - 25.0 GPa. The calculation of parameters of the ringwoodite occurrence in the experiment demonstrate, that σ_{xx} is not less than 22 - 28 GPa, and temperature is 1065 - 1256°C. STA in garnet in the Janisjarvi astrobleme composed by rhombic pyroxene, hercynite and sanidine. In the experiment, STA consist of hercynite, glass and, sometimes, ilmenite.

Thus, three conclusions should be drawn:

- STA are formed on an isentrope (as it was previously observed for other minerals);
- differences in natural and experimental STA in mineral associations, σ_{xx} and T° are the result of the quicker cooling of a rock in the laboratory, because of the smaller sizes of the impacted rock volume, and, as a consequence, of the earlier hardening; another reason of differences in natural and experimental STA are various chemical composition of rock in natural and phase diagrams in [8];
- fluid-containing character of the system in nature (as opposed to a "dry" experiment) can contribute to the decrease in T (and σ_{xx} of the STA formation in nature.

References:

- [1] Geology of Astroblems (1980), 231p. (In Russian). [2] Impactites (1981), 240p. (In Russian). [3] Sazonova L.V. (1984), Petrography of Jnisiarvi Astrobleme Impactites. Phi. Doc. thesis, Moscow State University, 268p. (In Russian). [4] Fel'dman V.I., Sazonova L.V. (1988), Meteoritics, 47, 197 - 205. (In Russian). [5] Fel'dman V.I. (1990), Petrology of Impactites, 299p. (In Russian). [6] Sazonova L.V. et al. (2000), METEORITE IMPACTS IN PRECAMBRIAN SHIELDS, Abstract p.91. [7] Kozlov E.A. (1999), Russian Federal Nuclear Center - E.I.Zababakhin Research Institute of Technical Physics, V Zababakhin Scientific Talks, Part II, p.413 - 424. (In Russian). [8] Ehlers E.G. Interpretation of Geological Phase Diagrams (1972), 298p. [9] Shock Craters on Moon and Planets (1983), 200p. (In Russian). [10] Kozlov E.A. et al. (2003), Doklady RAS, vol. 390, N 3. (In Russian).

CHEMICAL DIFFERENTIATION OF IMPACT-PRODUCED MELT DROPLETS: EXPERIMENTS AND OBSERVATION.

M. V. Gerasimov¹ O. I. Yakovlev², Yu. P. Dikov³, and F. Wlotzka⁴. ¹Space Research Institute, RAS, Moscow 117997, Profsoyuznaya st., 84/32, mgerasim@mx.iki.rssi.ru, ²Vernadsky Institute of Geochemistry and Analytical Chemistry, RAS, Moscow 117975, GSP-1, Kosygin st., 19, yakovlev@geokhi.ru, ³Institute of Ore Deposits, Petrography, Mineralogy and Geochemistry, RAS, Moscow 109017, Staromonetny per., 35, dikov@igem.ru, ⁴Max-Planck-Institut für Chemie, Abteilung Kosmochemie, Mainz, Germany.

Introduction: The main problem of the relation of ejected melted spherules and target rocks in impact structures is the unknown degree of their differentiation during the high-temperature stage. An investigation of trends of chemical differentiation of melted droplets during impact simulated processes can give a certain evidence for correlation between melt and target rocks in impact sites. Here we present experimental data on impact-simulated vaporization of obsidian that helps to reveal vaporization signatures in impact glasses formed from acidic and intermediate composition targets.

A certain problem for the relating of melt spherules and target rocks is the mixing of target rocks and projectile material. The formed spherules can represent a continuous row of mixed compositions which is modified by volatilization of elements during high temperature processing.

Experimental technique: Impact-simulation experiments were performed using a laser pulse (LP) technique [1]. Glass spherules with diameters ranging from around one to several tens of microns were found on the surface of the condensed film, which was precipitated on a Ni-foil at ~8 cm from the sample. Chemical analyses of spherules were performed using FESEM/EDS microprobe analyses.

Obsidian composition was (wt.%): SiO₂ 57.90; TiO₂ 1.32; Al₂O₃ 15.02; FeO 9.31; MgO 5.11; CaO 7.37; Na₂O 2.99; K₂O 0.53. We have analyzed 83 glass spherules and 10 microareas on polished cross-sections of glass remnants on the walls of the laser-produced crater. Results of analyses were statistically treated and compared with composition of the starting obsidian.

Results: Figures 1 and 2 show negative correlation trends between concentrations of moderately volatile Na and Si and refractory Al in glass spherules. These figures show an increase of Al and decrease of Si and Na concentrations in spherules and in the crater glasses in comparison with that of the starting obsidian. The crater glasses have smaller compositional differentiation than spherules what indicates that they were formed at lower temperatures. Crater glasses have higher K/Na ratio compared with that in the starting obsidian (Fig. 3). This is due to different K and Na

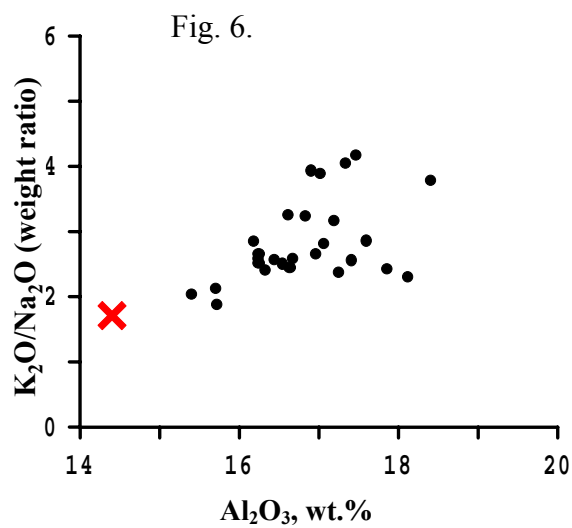
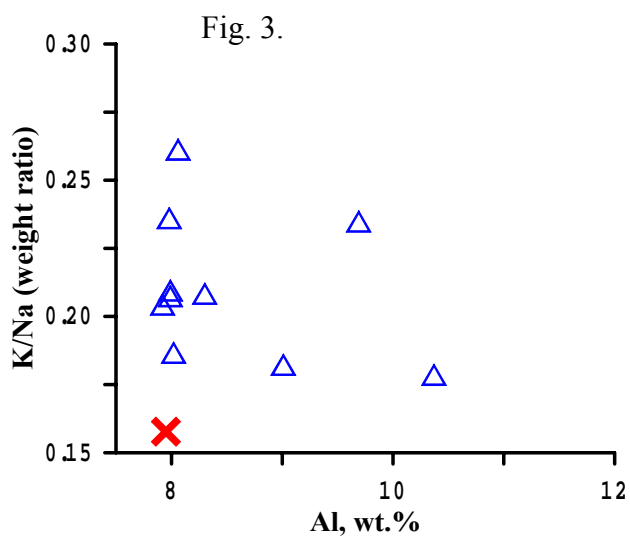
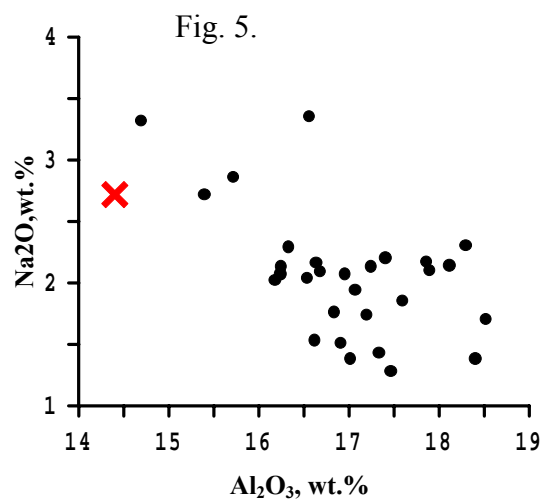
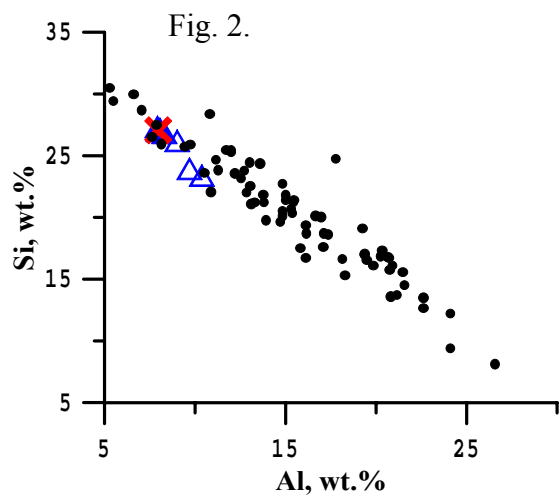
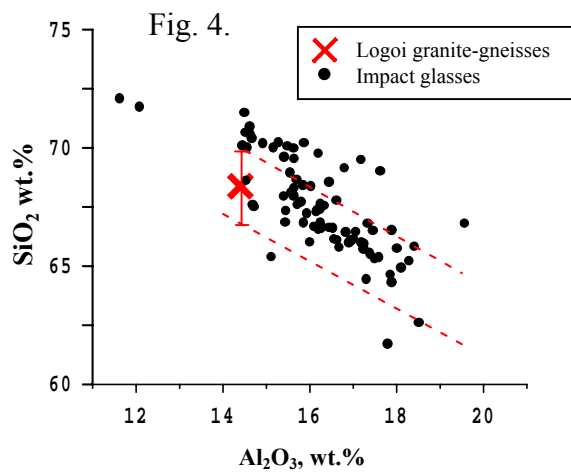
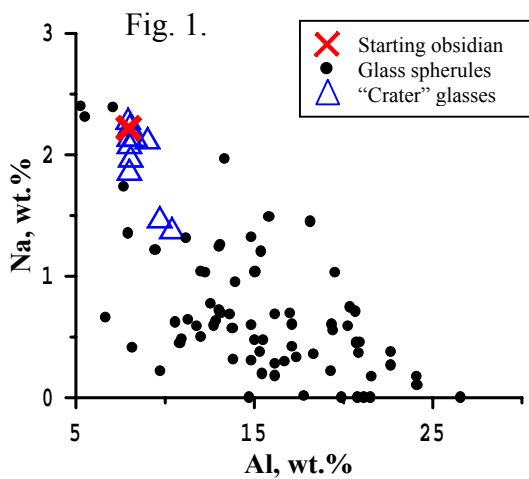
vaporization rates that is typical for acidic and intermediate composition melts [2].

The Logoi impact glasses: We tried to identify vaporization effects in natural impact glasses from the Logoi crater (D≈10 km; Belorussia) [3]. The target is a two-layer structure with sandstones overlying granite-gneisses. Impact glasses here were mainly resulted from granite-gneiss melting. Fig. 4 shows the SiO₂ and Al₂O₃ anti-correlation in homogenized impact glasses and values for the average composition of the target granite-gneisses.

Compared to a rather strict anti-correlation of Al and Si for experimental spherules (Fig. 2) Logoi glasses show a wider dispersion of Si vs. Al points (Fig. 4). This can be the result of inhomogeneity of the target rocks and/or mixing of gneisses and sandstones. An approach was suggested to derive a uniform population from Logoi glass compositions by an application of strict experimental trend (Fig. 2). This population is limited within dashed lines (Fig. 4) starting at target granite-gneisses compositions marked by an error bar. Fig. 5,6 demonstrate Na-Al and K/Na-Al correlation trends for impact glasses from the chosen composition field of Fig. 4. On the whole these trends are similar to the experimental ones that confirms the validity of such approach. This approach was also supported by other elements trends also for impact glasses from other craters. The selection of uniform glass populations can also be derived by an application of other strict ratios, e.g. Ca/Al ratio [4].

References: [1] Gerasimov M.V. et al. Physics and chemistry of impacts // In: Laboratory Astrophysics and Space Research. 1999. pp.279-329. Kluwer Academic Publishers. [2] Yakovlev O.I. et al. K and Na vaporization from melts. Vestnik MGU. 1973. N5. pp.85-88. (in Rus.) [3] Glazovskaya L.I. et al. The Logoi Astrobleme. 1991. M. Nauka. 134 p. (in Rus.) [4] Gerasimov, M.V., et al. LPSCXXII, 1991, pp. 437-438.

Acknowledgment. This research was supported by the RFBR grant 01-05-64564.



NEW DATA ON THE LATE PLIOCENE ELTANIN IMPACT INTO THE DEEP SOUTHERN OCEAN

Rainer Gersonde¹, Frank T. Kyte², T. Frederichs³, U. Bleil³, and Gerhard Kuhn¹. ¹Alfred Wegener Institut für Polar- und Meeresforschung, Postfach 120161, D-27515 Bremerhaven, Germany (rgersonde@awi-bremerhaven.de). ²Center for Astrobiology, Institute of Geophysics and Planetary Physics, University of California, Los Angeles, CA 90095-1567, USA (kyte@igpp.ucla.edu). ³Earth Science Department, University of Bremen, Postbox 330440, Bremen, 28334.

The late Pliocene impact of the Eltanin asteroid is the only known asteroid impact in a deep-ocean (~5 km) basin. This was first discovered in 1981 as an Ir anomaly in sediment cores collected by the USNS Eltanin in 1965[1]. The expeditions ANT-XII/4 (1995) and ANT-XVIII/5a (2001) of the *RV Polarstern* collected extensive bathymetric and seismic data sets as well as sediment cores from an area in the Bellingshausen Sea (eastern Pacific Southern Ocean) that allow the first comprehensive geoscientific documentation of an asteroid impact into a deep ocean (~5 km) basin, named the Eltanin impact[2-5]. Impact deposits have now been recovered from a total of more than 20 sediment cores (including up to 17 cores from the 2001 expedition) collected in an area covering about 80,000 km². Sediment texture analyses and studies of sediment composition including grain size and microfossil distribution reveal the pattern of impact-related sediment disturbance and the sedimentary processes immediately following the impact event. The pattern is complicated by the Freeden Seamounts (~57.5 S, 90.5 W; we previously called these the San Martin Seamounts, but they were officially named Freeden in 1999), a large topographic elevation that rises up to 2700 m above the surrounding abyssal plain in the area affected by the Eltanin impact. The impact ripped up sediments as old as Eocene and probably Paleocene that have been redeposited in a chaotic assemblage. This is followed by a sequence sedimented from a turbulent flow at the sea floor, overprinted by fall-out of airborne meteoritic ejecta that settled through the water column. Grain size distribution of reworked sediments and ejecta reveals the timing and interaction of the different sedimentary processes.

One of the most remarkable characteristics of this impact deposit is the high concentrations of melted and unmelted meteoritic material [6] distributed across a large area of ocean floor. We estimate the total amount of meteoritic materials by measuring bulk Ir concentrations in the sediment (using 187 ng/g as the concentration of Ir in the meltrock and the precursor asteroid [7]), and by measuring the amount of meteoritic ejecta in the coarse fractions of the sediment. Such measurements of the original USNS Eltanin cores provided a 500 m estimate for the minimum asteroid diameter. Using data from the 1995 Polarstern expedition, Gersonde et al. [2] found this was too conservative and recommended a minimum diameter of 1 km. With the much greater areal

coverage and large number of sediment cores from the recent expedition, we will be able to greatly refine the model for ejecta distribution. To date we have measured Ir concentrations in sediments from 11 of the new cores. Our initial interpretation of these data is that there is a region in the vicinity of the Freeden Seamounts comprising at least 20,000 km² in which the average amount of meteoritic material deposited was > 1 g/cm² (two sites have > 6 g/cm²). This alone is enough material to support a 500 m asteroid. Beyond this is a region of about 60,000 km², mostly to the north and east, where the amount of ejecta probably averages about 0.2 g/cm². Another 400 km to the east, USNS Eltanin core E10-2 has about 0.05 g/cm², so we know that coarse ejecta probably occurs across more than 10⁶ km² of ocean floor. A key to future exploration of this impact is to find evidence of the ejecta at sites more distant from the seamounts. We currently have almost no data from regions to the west or south of the Freeden Seamounts, but sediment cores documenting the impact time interval collected at distant locations are now being studied.

At least one site (PS58-281, just north of the seamounts) has more than 8 g/cm² of meteoritic ejecta. Near the top of 8.5 m of impact deposit in this core, this ejecta is interbedded with disturbed sediments in a graded unit more than 50 cm thick. One 2.5 cm interval has 150 ng/g Ir, or about 80% meteoritic ejecta, by weight. One 2.5 cm meteorite has been recovered and 10 g of meteoritic ejecta (0.5 to 8 mm) has been examined. Of this, 87% is asteroidal meltrock and 13% is meteorite fragments. Unmelted meteorites are most concentrated in the lower part of the ejecta-bearing sediments, consistent with their greater density, and thus more rapid settling time through the 5 km water column, relative to the vesicular meltrock. In this particular core, which is 8 cm in diameter, we estimate that we recovered in excess of 500 g of melted and unmelted asteroid material. This is clearly the most meteorite-rich region known on the surface of the Earth.

The impact was formerly dated to about 2.15 Ma [2]. This estimate was based on regional analyses of the geological record combining bathymetric and seismic surveys with detailed sedimentologic and geochemical (e.g., chromium and iridium anomalies), biostratigraphic (diatoms and calcareous nanofossils) and principally on magnetostratigraphic studies of sedimentary deposits recovered in 3 piston cores. Only one of them apparently contained an adequately

complete and continuous late Pliocene sequence, however, whereas a hiatus spanning major parts of the Matuyama Chron was encountered in the other two cores. The age assignment therefore essentially relied on the identification of the magnetostratigraphic Réunion Event (C2r.1n) and the *Thalassiosira kolbei* - *Fragilariopsis matuyamae* diatom zone directly above the impact related deposits in a single core. New chronostratigraphic data have been obtained on a series of 4 piston cores retrieved during cruise ANT-XVIII/5a in the wider vicinity of the Eltanin impact area. Initial correlation of their magnetic susceptibility records with previous data sets substantiated the age estimate of the impact event in the early Matuyama Chron. High-resolution integrated magnetobiostratigraphic analyses provided convincing evidence, at least in two cores with high enough sedimentation rates in the critical interval, that the Eltanin impact not only predates the geomagnetic Réunion Event, but also the unnamed normal polarity event (C2r.2r-1) listed in the most recent Geomagnetic Polarity Time Scale. This finding would now constrain the Eltanin impact age to 2.511 ± 0.07 Ma, between the top of the Gauss Chron (2.581 Ma) and the base of the C2r.2r-1 event (2.441 Ma), a climate period that has been affected by major glaciations on the Northern hemisphere.

Our most recent results suggest that the Eltanin asteroid was larger than the 1 km in diameter size originally proposed as a minimum based on the ANT-

XII/4 results. This places the energy released by the impact at the threshold of those considered to cause environmental disturbance at a global scale and it makes the impact a possible transport mechanism explaining the presence of extinct Cenozoic microfossils in the transantarctic Sirius Unit. Although a crater structure representing Eltanin ground zero has not been discovered, the distribution pattern of sediment disturbance and ejecta deposits now allows us to better determine the central target area north of the Freedom Seamounts. The new age estimate of the impact places it at a time of rapidly fluctuating climate. One of our future goals is to correlate this impact to a high sedimentation rate site with an established oxygen-isotope stratigraphy. This would allow us to assess possible climatic effects of the impact event.

References: [1] Kyte, F. T., Zhou, Z., and Wasson, J. T. (1981) *Nature* 292, 417-420. [2] Gersonde et al. (1997) *Nature* 390, 357-363. [3] Gersonde et al. (2002) AGU Fall Meeting abs.# OS22C-0285. [4] Kyte et al. (2002) AGU Fall Meeting abs.# OS22C-0287. [5] Frederichs et al (2002) AGU Fall Meeting abs.# OS22C-0286. [6] Kyte, F. T., and Brownlee, D. E. (1985) *Geochim. Cosmochim. Acta* 49, 1095-1108. [7] Kyte F.T. (2002) *Deep Sea Res. II* 49, 1029-1047.

REPORTS OF DISCOVERY OF THE "ELTANIN CRATER" ARE CONTRADICTED BY DATA. Rainer Gersonde¹, Frank T. Kyte², T. Frederichs³, U. Bleil³, and Gerhard Kuhn¹. ¹Alfred Wegener Institut für Polar- und Meeresforschung, Postfach 120161, D-27515 Bremerhaven, Germany (rgersonde@awi-bremerhaven.de). ²Center for Astrobiology, Institute of Geophysics and Planetary Physics, University of California, Los Angeles, CA 90095-1567, USA (kyte@igpp.ucla.edu). ³Earth Science Department, University of Bremen, Postbox 330440, Bremen, 28334.

Deposits of the Eltanin impact event were first discovered as an Ir anomaly in deep-sea sediments of late Pliocene age deposited in the South-East Pacific Ocean [1] (Fig. 1). These were found to contain coarse ejecta composed of an Ir-rich melt rock derived directly from the impacting asteroid, and several percent unmelted meteorites, since named the Eltanin meteorite [2]. A 1995 *R/V Polarstern* expedition to the suspected impact region [3] found that sediments in the region around the Freeden Seamounts (57.3°S 90.5°W; we previously called these the San Martin Seamounts, but they were officially named Freeden in 1999) contained high concentrations of meteoritic ejecta – typically $\geq 1 \text{ g/cm}^2$. They also found that sediments in this region had been severely disrupted by the impact, which ripped-up and redeposited sediments as old as Eocene in age.

Two recent abstracts [4,5] claim possible identification of a submarine source crater for the Eltanin impact event. Although this is only described as a possible identification of a "prospective Eltanin crater," statements like "seismic lines show a clear ejecta blanket around the Eltanin Crater," and the presentation of these results make it clear that the authors consider this identification to be correct. This purported submarine crater is supposed to be 132 km in diameter and centered at 53.7°S 90.1°W (Fig. 1). In this abstract we wish to state categorically that our extensive study of the Eltanin impact event, including detailed exploration of the impact area and even a pass through the hypothetical crater show that these authors cannot possibly have found the Eltanin impact site.

We are currently working on core samples and geophysical data from a 2001 expedition, which includes up to 17 new sediment cores covering an area of $>80,000 \text{ km}^2$. We explored an area extending from ~ 55 to 58°S and 89 to 95°W , using bathymetric mapping, echosounding profiles of near-surface sediments, and sediment piston coring. Our initial results [6-8] show that disturbance from the impact clearly extends for about 100 km north and east of the Freeden Seamounts (Fig. 1). However, with increasing distance to the north and the east, the concentrations of ejecta decrease and thick deposits of disturbed sediments are not present. One core (PS58/294-1; 55.85°S , 92.12°W) was taken only 271 km from the

center of the purported "Eltanin crater" (Fig. 1). Here, we found undisturbed late Pliocene sediments. The ejecta deposit must have been thin as it was subsequently smeared by bioturbation as is normal in these sediments. Our preliminary results on this core show that only $\sim 0.1 \text{ g/cm}^2$ of meteoritic ejecta were deposited there, at least an order of magnitude less than is found in the disturbed region to the south. New data from extensive integrated magnetobiostratigraphic studies indicate that the impact occurred during the lowermost Matuyama Chron, a period of reversed magnetic polarity, at about 2.5 Ma.

Several lines of evidence argue against the hypothetical 132 km Eltanin impact crater. **First**, all our data indicate that the greatest disturbance and highest concentrations of meteoritic material are in the vicinity of the Freeden Seamounts. The physical disturbance and ejecta concentrations clearly decline quickly to the east and north (i.e., in the direction of the hypothetical crater); we have no significant data to constrain this to the west or south of the seamounts. The data appear to be most consistent with an impact in the region near the northern edge of the seamounts. **Secondly**, all our analyses of the impact ejecta indicate that the projectile did not even form a significant crater on the ocean floor. The bulk chemistry of the impact melt rocks is essentially that of the parent mesosiderite asteroid with an admixture of a few percent Na, K, and Cl derived from seawater salts [9]. There is no geochemical evidence to support the possibility that the asteroid was mixed with any significant fraction of sediments or basalt that would be in a typical ocean lithosphere target. We find it inconceivable that a deep ocean impact large enough to form a 132 km crater could avoid mixing of projectile and target. Even if there were no mixing, we expect that excavation of this crater would produce abundant terrestrial ejecta including considerable volumes of shocked basaltic rock from the oceanic lithosphere. No such materials have been identified in any of the 21 sediment cores examined to date. **Thirdly**, in our exploration of the region as far north as 55°S , we find no evidence of disturbed sediments near the purported crater. At site PS58/294, which is about two diameters from the center of the hypothetical crater (271 km), our core contains traces of meteoritic ejecta, consistent with an origin as distal ejecta from an impact near the Freeden

Seamounts. There is no evidence of disturbance or ejecta from terrestrial target material, which we should expect if there were a 132 km crater only a short distance to the north. **Finally**, and most significantly, during our 1995 expedition, we passed through the region of the hypothetical crater. Our echosounding profiles of near-surface sediments showed nothing unusual in the sediments in this region. We obtained the 17.72 m long piston core PS2664-1 (53°49'S, 89°34'W) only 37 km from the center of the proposed impact structure (Fig. 1). The upper 7.95 m consist of diatomaceous mud. Integrated geomagnetic and diatom biostratigraphic dating of this section indicates a continuous sediment record extending back into the late Gauss Chron, thus documenting the past ca. 2.7 Ma. No sediment and geomagnetic disturbance is visible at the interval in the lowermost Matuyama that corresponds to the age of the Eltanin impact, which definitely precludes the presence of a crater formed by the Eltanin impact in this region.

In summary, all credible data contradict the hypothesis that the Eltanin impact formed a 132 km crater at the locality proposed by [4,5]. We object to further use of the term "Eltanin crater" unless this can be proven undisputedly to be derived from the Eltanin impact. Although we consider it unlikely that the Eltanin impact formed a true crater, the impact might have formed a mapable structure on the ocean floor which we may find in future expeditions. We believe that the term "Eltanin crater" should be reserved for this possible future discovery.

References: [1] Kyte, F. T., Zhou, Z., and Wasson, J. T. (1981) *Nature* 292, 417-420. [2] Kyte, F. T., and Brownlee, D. E. (1985) *Geochim. Cosmochim. Acta* 49, 1095-1108. [3] Gersonde et al. (1997) *Nature* 390, 357-363. [4] Glatz C.A., Abbott D.H., and Nunes A.A. (2002) *GSA Abs. Prog.* v. 34, No 6, p. 401. [5] Abbott D.H., Glatz C.A., Burckle L., and Nunes A.A. (2003) *LPSC XXXIV abs.* # 1858. [6] Gersonde et al. (2002) *AGU Fall Meeting abs.*# OS22C-0285 [7] Kyte et al. (2002) *AGU Fall Meeting abs.*# OS22C-0287 [8] Frederichs et al (2002) *AGU Fall Meeting abs.*# OS22C-0286. [9] Kyte F.T. (2002) *Deep Sea Res. II* 49, 1029-1047.

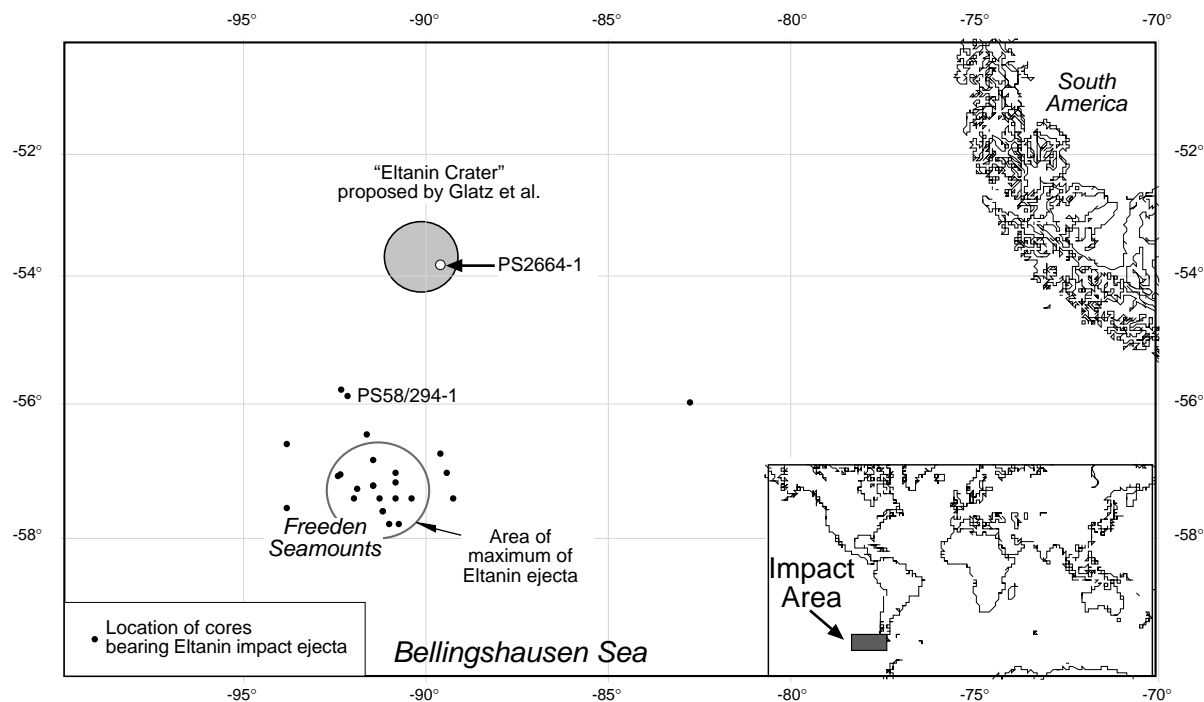


Fig. 1. Location of sediment cores bearing Eltanin impact ejecta in the South-East Pacific Ocean and the hypothetical 132 km "Eltanin crater" purported by [4, 5]

VREDEFORT 2003 – RECENT PROGRESS, NEW CHALLENGES. R.L. Gibson, W.U. Reimold, and C. Lana, Impact Cratering Research Group, School of Geosciences, University of the Witwatersrand, P O WITS, Johannesburg 2050, South Africa, gibsonr@geosciences.wits.ac.za, reimoldw@geosciences.wits.ac.za, lanac@science.pg.wits.ac.za.

Introduction: The Archean and Paleoproterozoic rocks of the Witwatersrand region in South Africa preserve a unique deep section through the giant, 2.02 Ga, Vredefort Impact Structure. This paper outlines some of the advances made in the last 5 years in understanding the nature of the impact processes that affected these rocks, and some of the ongoing work and outstanding challenges that remain. Field and petrographic research has centered on the ~80-km-wide central uplift of the structure (the Vredefort dome), which exposes a 35-40 km wide early Archean crystalline basement core and surrounding 15-20 km wide collar of steeply-dipping younger supracrustal strata. Research in the outer parts of the impact structure has been largely restricted to petrographic work on the gold-bearing strata of the Witwatersrand basin aimed at understanding impact-induced thermal effects in the crater basement. The absence of crater-fill impact melt rock and other breccias confirms the deep level of erosion of the structure, which is estimated at between 5 and 10 km [1-3].

Large-scale structure: Recent structural and lithological studies in the crystalline basement rocks in the core of the Vredefort dome [4,5] have challenged earlier interpretations (e.g., [6]) that the central uplift exposes lower crust and uppermost mantle within its core. The rocks in the core of the dome and their metamorphic grade are consistent with mid-crustal levels of exposure, and the structural data indicate decreasing amounts of impact-induced rotation towards the center [5]. Lana et al. [5] have demonstrated that the present asymmetry of dips in the collar strata (overturned in the northwestern sector, right-way-up in the southeastern sector) can be reconciled with symmetric impact-induced rotation of an inclined pre-impact supracrustal sequence, rather than asymmetric central uplift processes. Whilst the dome is cut by a variety of faults of impact origin, there is little evidence of chaotic block rotation (“megabreccia structure”) as has been identified at shallower levels of other large impact structures. Fracture analysis by Wieland et al. [7] suggests that most of the joints in the collar rocks are the likely result of radial and tangential collapse of the central uplift. In the absence of any evidence of small-scale ductile features associated with central uplift formation, the role of the pervasive pseudotachylite vein-fracture network in accommodating strain during the post-impact crater modification stage is currently being investigated (see below). Extensive

mapping of macroscopic occurrences of pseudotachylitic breccia in the core region has been carried out and is reviewed by [8].

Shock deformation: Outside of the limited work done by Stepto [9] and Schreyer and co-workers [10,11], impact-related effects in the rocks in the central parts of the core of the dome have received little attention, mainly because of poor exposure, but also because of extensive post-impact metamorphic overprinting [3,9]. A recent study of a 200-m-long borehole section drilled 4 km south of the geographic center of the dome has provided new impetus to petrographic studies of these rocks. A range of shock effects in feldspars, biotite, amphibole, pyroxene and zircon have been identified [3]. These indicate that peak shock pressures do, indeed, show a systematic increase towards the center of the dome, but that significant outcrop-scale variation also exists. Although post-shock thermal effects obscure the shock effects to varying extents, evidence of diaplectic glass formation and melting in feldspars suggest peak shock pressures exceeded 30 GPa, and may have reached 40-45 GPa, in the central parts of the structure [3,12]. Within 7 km of the center, however, mineral textures are consistent with background shock pressures of <15 GPa. The broad concentric distribution of shock isobars, but local complexity in maximum shock pressure values, agree with studies of the central uplifts of less-exhumed complex craters (e.g., [14]).

Petrographic analysis of pseudotachylitic breccias from the dome has revealed what appear to be annealed shock features preferentially developed in mineral grains along the margins of thin veins. Such veins also show continuity with thicker veins previously classified as “B-type” veins of endogenous origin [15]. This may indicate that much, if not all, of the pseudotachylitic breccia in the dome formed by shock melting in response to localized elevation of shock pressures caused by reflection and refraction of the shock wave through the heterogeneous target rocks. Whilst veins commonly show evidence of millimeter-scale offsets, indicating that frictional heating may have played a role, it is also possible that slip occurred after formation of the melts, during the crater modification phase, when melt-lubricated fractures would have assisted differential movement between blocks. Stresses related to crater modification could then have expelled melts from the generation sites into tensional sites, thereby forming larger veins and dykes. Whilst these findings

challenge the traditional “A-type and B-type pseudotachylite” classification within the central uplift, per se, frictional heating related to crater collapse faults remains the only plausible mechanism to explain the voluminous pseudotachylites occurring beyond the dome in the wider Witwatersrand basin.

Post-shock thermal processes: The deep levels of erosion in the Vredefort impact structure mean that heat derived from shock pressure decay and the uplift of mid-crustal rocks in the central uplift was lost much more slowly than would occur at shallower levels. This allowed sufficient time for extensive annealing of shock features, and even metamorphic reactions, to occur. Whilst the former is a problem for the identification of shock features, the latter has provided constraints on post-shock P-T conditions and on the post-shock temperature distribution across the dome [3,12]. The entire basement to the crater appears to have experienced a low-grade, ca. 300 °C, hydrothermal overprint related to the impact event [3]. In the dome, however, post-shock temperatures increase from 300 °C at a radial distance of 25 km from the center, to ~700 °C some 7 km from the center. This is deduced from retrograde assemblages that overprint higher-T pre-impact metamorphic assemblages and the shock effects. In the center of the dome, however, post-shock temperatures actually exceeded the peak (granulite-facies) pre-impact metamorphic temperatures, ranging from at least 900 °C to nearly 1400 °C (as deduced from melting of feldspar) [12]. These exceptional temperature conditions led to local anatexis of the basement gneisses (which had already experienced early Archean anatexis) to produce small granite veins and bodies (including the so-called Central Anatectic Granite) [12,16]. Unusual granulitic-textured breccias found in the central parts of the dome are interpreted as annealed shock ± friction melts. These have been compared to granulites obtained from the Moon and may provide an explanation for the latter which have previously been interpreted as contact-metamorphosed impact breccias [12].

Economic implications: Petrographic studies of gold reefs in the Witwatersrand Supergroup exposed in the collar of the Vredefort dome and in the mines some 80-100 km from the center of the dome have established that much of the microscopically-visible gold in the reefs, which is believed to be of original placer origin, was precipitated or recrystallized after the Vredefort impact event [17]. We interpret this as evidence for the existence of a massive hydrothermal system in the fractured crater basement following the impact. Widespread resetting of sericitic mica K-Ar and Ar-Ar systematics within the Witwatersrand basin at 2.02 Ga [18-20] supports this. The heat source for the hydro-

thermal system is believed to be the uplifted, shock-heated central uplift, and the overlying superheated impact melt sheet and breccias [21].

Current work and new challenges: Research is currently focused on the structures within the collar of the Vredefort dome, aimed at further constraining the structural evolution of the central uplift. Additional work is being conducted on pseudotachylitic breccia genesis and thermal history. The extensive multi-disciplinary data base for the Vredefort-Witwatersrand region should provide an excellent basis for comprehensive modeling of this giant impact event. Remote sensing analysis of the wider Witwatersrand region is planned. Further work is needed on the structure of the surrounding region, making use of the extensive seismic data base for the Witwatersrand region and structural geological data from mining companies.

References: [1] McCarthy, T.S. et al., 1990, *S. Afr. J. Geol.* 93, 1-4; [2] Henkel, H. & Reimold, W.U., 1998, *Tectonophysics* 287, 1-20; [3] Gibson, R.L. et al., 1998, *Geology* 26, 787-790; [4] Lana, C. et al., 2003, *EPSL* 206, 133-144; [5] Lana, C. et al., 2003, *MAPS*, in revision; [6] Hart, R.J. et al., 1990, *Chem. Geol.* 82, 233-248; [7] Wieland, F. et al., 2003, this volume; [8] Dressler, B.O. & Reimold, W.U., *Earth-Sci. Rev.*, in revision; [9] Stepto, D., 1990, *Tectonophysics* 171, 75-103; [10] Schreyer, W., 1983, *J. Petrol.* 24, 26-47; [11] Schreyer, W. & Abraham, K., 1978, *CMP* 68, 53-62; [12] Gibson, R.L. et al., 2002, *Geology* 30, 475-478; [13] Gibson R.L., 2002, *J. met. Geol.* 20, 57-70; [14] Dressler B.O. et al., *Geol. Soc. Amer. Spec. Pap.* 339, 109-124; [15] Martini J.E.J., 1991, *EPSL* 103, 285-300; [16] Gibson R.L. et al., 1997, *GCA* 61, 1531-1540; [17] Foya S.N., 2002, *Mineralogical and chemical controls on gold distribution in the Kimberley Reefs, South Africa*, PhD Thesis, Geosciences, Univ. Witwatersrand, Johannesburg; [18] Layer, P.W. et al., 1988, *JGR* 93, 2191-2200; [19] Trieloff, M. et al., 1994, *S. Afr. J. Geol.* 97, 365-384; [20] Gibson R.L. et al., 2000, *S. Afr. J. Geol.* 103, 175-190; [21] Gibson R.L. & Reimold W.U. (1999) *Miner. Petrol.* 66, 5-23.

MAGNETIC FABRIC STUDIES OF THE WHISTLE AND PARKIN OFFSET DYKES FROM THE SUDBURY IMPACT STRUCTURE. L. A. Giroux¹ and K. Benn², Ottawa-Carleton Geoscience Centre and University of Ottawa, Department of Earth Sciences, 140 Louis Pasteur, Ottawa, Ontario, Canada K1N 6N5, ¹lgro564@science.uottawa.ca, ²kbenn@uottawa.ca

Introduction: Quartz-diorite Offset dykes from the 1.85 Ga Sudbury Impact Structure stem from the Sudbury Igneous Complex (SIC) and extend into the footwall rocks of the impact structure, forming radially and concentrically arranged intrusions. The dykes represent impact-generated magmas emplaced into radial and concentric fractures that were generated in the country rock by the hypervelocity impact [1]. The Parkin and Whistle Offset dykes are located to the northeast of the SIC. The Parkin Offset dyke may be a faulted extension of the Whistle Offset dyke.

Objectives: The present research is aimed at mapping fabrics (bulk mineral preferred orientations) and subfabrics (preferred orientations of distinct populations of minerals), within the Whistle and Parkin Offset dykes. The fabrics and subfabrics may record flow patterns during emplacement of the intrusions, and they may also provide important information on the formation of economic deposits of Cu, Ni and PGEs that are hosted by the Offset dykes. The fabrics and subfabrics are measured using two magnetic anisotropy methods. A previous study showed that the radial Copper Cliff Offset dyke acted as a melt-lubricated fault during collapse of the inner rim of the impact crater and that the flow pattern in the dyke controlled the elongate shapes of the mineral deposits [2,3].

Methods: Two magnetic anisotropy methods are employed which allow the preferred orientations of crystals to be measured within oriented core samples collected from the Whistle and Parkin Offset dykes. The mineral fabrics may record the symmetry of flow of magma thereby recording the emplacement of the Offsets, and possibly shedding light on the origins of the sulphide deposits they host.

AMS. The first technique, the anisotropy of magnetic susceptibility (AMS), measures the bulk fabric of all iron-rich minerals in the samples. It involves placing a 10 cm³ specimen within a weak magnetic field. The magnetic susceptibility (K) is measured in several predefined orientations so that an AMS tensor can be defined for each specimen, and an average tensor can be calculated for each sampling site. AMS is an efficient method and has previously been used to study dykes in the Sudbury camp [2,3].

ApARM. The second technique, the anisotropy of partial anhysteretic remanent magnetization (ApARM), involves the cleaning of all natural magnetic remanence from a specimen by subjecting it to a slowly decaying alternating field. A new (partial) an-

hysteretic remanence is imparted in a predefined orientation by subjecting the specimen to a similarly decaying alternating field with a superimposed, co-axial direct bias field that is applied during part of the decay cycle of the alternating field. Measurements of the anisotropy of remanence applied in several orientations provide the data for a second-order tensor (ApARM) similar to the AMS, but which only records the fabrics defined by the ferromagnetic minerals, pyrrhotite and/or magnetite. By choosing the proper "window" of application of the direct field during decay of the alternating field, it is possible to separate the fabrics defined by pyrrhotite from those defined by magnetite, as well as the fabrics defined by different grain size populations of the same mineral [4]. This allows us to document and analyze the fabrics of different mineral populations (subfabrics) in order to separate the signals from "primary" minerals that formed during the emplacement of the dyke from those of "secondary" minerals that formed during the later metamorphism and hydrothermal alteration of the rocks.

Results: Results are presented for different lithologies from both the Whistle and Parkin Offsets, including quartz diorite, massive sulphide samples and strongly hydrothermally altered rock. Results obtained using the AMS and the ApARM are compared and the definition of subfabrics for different mineral populations is demonstrated. The results are then considered in the context of petrographical and petrological studies to develop a model for the emplacement of the impact-generated magmas as radial dykes. We also discuss constraints placed by the results on models for the formation of the hosted ore deposits.

References: [1] Grant, R.W., and Bite, A. (1984) *Ont. Geol. Surv. Spec. Vol. 1*, 275-301. [2] Scott, R.G., and Benn, K. (2001) *Geology*, 29, 747-750. [3] Scott, R.G., and Benn, K. (2002) *Econ. Geology*, 97, 1447-1458. [4] Jackson, M. (1991) *Pure and Applied Geophysics*, 136, 1-28.

ACTIVE SEISMIC AND DRILLING STUDIES OF THE CHICXULUB IMPACT

CRATER: A STATUS REPORT. S. P. S. Gulick¹, G. L. Christeson¹, J. V. Morgan², M.R. Warner², P. Barton², J. Urrutia-Fucugauchi³, and H.J. Melosh⁴, ¹Univ. of Texas Inst. for Geophysics, 4412 Spicewood Springs Rd Bldg 600, Austin, TX 78759 USA, sean@ig.utexas.edu, ²T.H. Huxley School, Imperial College, Prince Consort Rd., London, SW7 2BP, UK, ³Instituto de Geofísica, UNAM, ciudad Universitaria, Mexico City, CP 04510, Mexico, ⁴Department of Planetary Sciences & Lunar and Planetary Laboratory, Univ. of Arizona, 1629 E. University Blvd., Tucson, AZ 85721 USA.

Introduction: The 65 Ma Chicxulub impact structure (Fig. 1) in Mexico is the largest Phanerozoic impact crater known on the Earth and likely records one of the more significant events in Earth history. Burial beneath ~1 km of Tertiary carbonates has preserved the crater in a uniquely pristine condition, where it is amenable to detailed investigation by drilling and surface geophysics. The Chicxulub crater was the focus of many past international efforts and is the focus of recent and upcoming efforts including continental (ICDP-1) drilling in 2002, future integrated ocean drilling program (IODP) drilling, and a combined 3D onshore-offshore tomographic study and 2-D/2.5-D seismic reflection survey planned for Spring 2004.

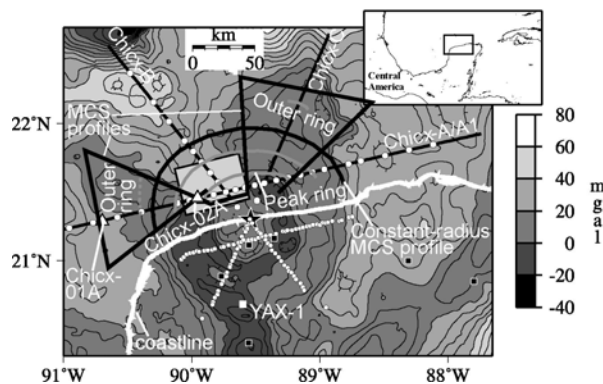


Figure 1. Gravity map of Chicxulub impact crater (courtesy of A. Hildebrand and M. Pilkington) showing location and layout of 1996 seismic program and planned 2004 MCS experiment. Coastline is delineated by the white line, center of crater is shown as a black star, and locations of onshore wells are marked by black squares. The white square shows the ICDP borehole (Yax-1), and white triangles mark the proposed IODP drill sites Chicx-01A and Chicx-02A. Inset shows location relative to the Yucatan Peninsula and Central America. Gray lines are locations of peak ring, crater rim, and outer ring as observed on existing MCS profiles. Shaded box shows location of UK 3D tomographic survey in Fig. 2.

Previous Work: These recent and planned geological and geophysical studies build upon previous studies including gravity surveys, seismic profiling, impact crater modeling, and industry drilling. In 1996 a combined seismic reflection/refraction experiment (Fig. 1) provided new constraints on the size and structure of the crater [1]. Major observations from these profiles are shown in Figure 2 and include the

morphology of the peak ring, slumping on normal faults, position of the crater rim, vertical offset across the outer ring, and the destruction of the Cretaceous stratigraphy. An irregular, rugged peak ring was imaged that stands a few hundred meters above the basin floor with an average diameter of 80 km. The profiles also showed 3-5 km of slumping from the crater rim towards the center of the crater that occurred along a single fault or a sequence of faults on all profiles. The crater rim was shown to average 130 km in diameter. Further outward from the crater's center an outer ring with an averaged diameter of 195 km exhibited 400-500 m of total vertical offset of the Cretaceous stratigraphy observed on two profiles. This offset exists either entirely across a monocline or straddling a monocline and a fault-bounded asymmetric graben. The outer ring appears to be related to bands of dipping, linear reflections in the crystalline crust that dip towards the crater center. At one location the reflections appear to offset the Moho by ~1 s (3-4 km). The images suggest that immediately after impact, there were two distinct inward-facing asymmetric scarps (the crater rim and outer ring) demonstrating that Chicxulub is a multi-ring crater. Inward of approximately 85 km diameter, no intact Cretaceous stratigraphy is observed, providing constraints on excavation cavity and transient cavity size. Restoring the slumped blocks to their pre-impact positions and reconstructing the transient rim uplift gives an estimate of 90-105 km for the diameter of the transient and excavation cavity. Scaling laws [2] place the maximum depth of excavation at 12 km and the depth of the transient cavity (with respect to the uplifted crater rim) at 35-40 km.

Recent and Upcoming Studies: Efforts to drill into the crater include the recent ICDP onshore drilling which cored ~100 m of impact breccia and IODP offshore drilling. Offshore IODP drilling at Chicxulub is one of the top four Mission Specific Platform (MSP) proposals and is expected to be scheduled for drilling early in the new program. ODP/IODP proposal 548-Full suggested two drill sites (Fig. 1 and 2). Chicx-01A would drill 4.3-km-deep borehole just outside the crater, in order to penetrate the Tertiary section, the proximal ejecta blanket, the entire Mesozoic section, and the Paleozoic basement rocks. Principal objectives of this borehole are to identify the thickness, composition, and character of the target rocks and proximal ejecta. Chicx-02A is a 3-km-deep borehole, which proposes to penetrate the peak

peak ring within the impact basin. Principal aims of this borehole are to determine the composition of the peak ring, test models of peak-ring formation, constrain the mechanism of transient cavity collapse that forms the final crater, and to use this information to improve estimates of crater size. Drilling at the shallow-water Chicxulub sites would be part of the post-2003 IODP multi-platform operation and is tentatively planned for 2005. The UK seismic program is, in part, a response to the recommendation by the science advisory panels that high-resolution 3D seismic tomography over the peak ring will be important for final drill-site selection and for understanding the sub-surface structure once drilling has occurred at Chicx-02A.

The UK-funded 3D tomographic experiment will collect onshore-offshore wide-angle data covering the northwest quadrant of the crater (Fig. 2). The UK teams will conduct a 3D tomographic survey over the northwest quadrant of the Chicxulub impact crater; embedded within the 3D tomographic survey will be a smaller, high-resolution tomographic survey centered over proposed IODP drill site Chicx-02A. The program will take place on the R/V *Ewing* in 2003, and will use the *Ewing* airgun array to shoot to a grid of OBS and land-based receivers. The planned 3D tomographic survey will consist of 40-60 OBS receivers (2 deployments of 20-30 instruments) in a staggered grid with resulting OBS instrument spacing of ~5 km (Figure 4); 100-150 land stations will record all shots. Shot spacing along the lines will be 50 m and cross-line spacing will be 3.75 km. The planned high-resolution survey will use 20-30 OBS instruments at a spacing of ~3.75 km, with 24 air gun profiles at a shot spacing of 50 m and a cross-line spacing of 1.875 km (Figure 4). The UK seismic program will map features critical to our understanding of large crater formation and the KT impact that were not sufficiently resolved by the larger-scaled reconnaissance study of 1996, and will undoubtedly map out new unknown features of the Chicxulub impact crater.

NSF-ODP recently funded a collaborative seismic reflection imaging (Fig. 1) and modeling program to: 1) acquire four new regional deep reflection profiles crossing through the proposed IODP drill sites Chicx-01A and Chicx-02A, 2) collect a pseudo-3D MCS survey during data acquisition of the UK tomographic survey, and 3) conduct 3D numerical modeling of the impact. Our goals are fourfold. First, we seek to determine the direction of approach and angle of the Chicxulub impact through the collaborative seismic and modeling effort. Experimental and numerical modeling studies show that vaporization depends on impact angle, with oblique impacts resulting in as much as a 15-20 fold increase in vapor production. Thus any constraints we can place on the obliquity of the Chicxulub impact will help quantify the amount of volatiles released into the atmosphere by the K-T event. Second, we will map the deformation recorded in the upper crust near the crater center that has previously been

poorly imaged and cannot be properly imaged with tomographic data. Third, by imaging the peak ring and other morphologic features in the northwest quadrant of the crater we can further understand the physical parameters of the Chicxulub impact structure and in doing so complete the site survey requirements for the IODP holes. Fourth, we intend to model the 3D collapse of an asymmetric transient crater. This modeling will not only help us better understand the mechanics of large impact craters, but will also quantify many of the environmental effects of the KT impact. The combined results of this proposed work, together with the UK tomographic experiment and the continental and oceanic drilling should significantly expand our understanding of the KT impact and by extension other large-diameter bolide impacts on Earth and our neighboring rocky planets.

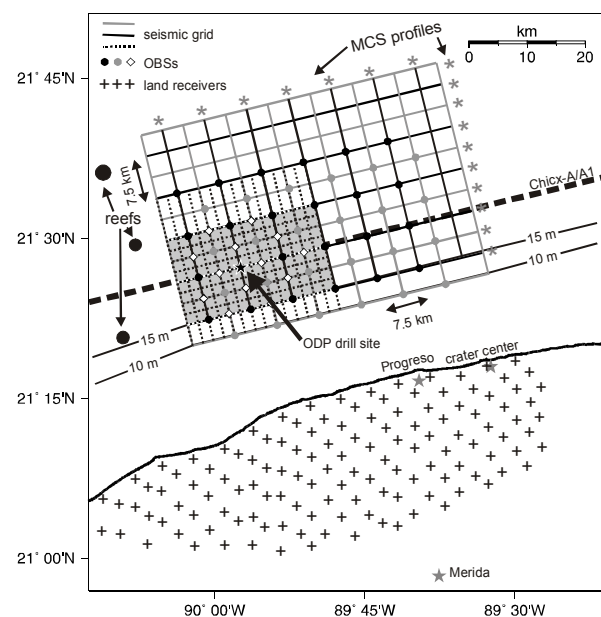


Figure 2. Planned UK-US-MEXC seismic program over the peak ring, consisting of nested MCS-OBS survey centered at IODP drill site Chicx-02A. Current plan is to 1) deploy 40-60 OBSs (circles and diamonds, 2 deployments of 20-30 instruments) within a 52.5x37.5 km grid, with air gun profiles at a cross-line spacing of 3.75 km, and to 2) deploy 20-30 OBS (circles and diamonds in gray shaded region) within a 26.25x15 km grid, with air gun profiles at a cross-line spacing of 1.875 km. Approximately 100-150 land receivers will record all shots (see Fig. 1). Coincident MCS data will be shot along the seismic profiles marked with the gray asterisks.

References:

- [1] Morgan, J., Warner, M., and the Chicxulub Working Group (1997) *Nature*, 390, 472-476,
- [2] Melosh, H.J. (1989), *Oxford monographs*, 11, Oxford University Press.